

# MODELLING MANUFACTURING DEFORMATIONS IN CORNER SECTIONS MADE OF COMPOSITE MATERIALS

*Kenan Çınar, Umud Esat Öztürk<sup>3</sup>, Nuri Ersoy<sup>1</sup>, Michael R. Wisnom<sup>2</sup>*

*<sup>1</sup>Bogazici University, Mechanical Engineering Department*

*TR-34342 Bebek, Istanbul, TURKEY*

*<sup>2</sup>University of Bristol, Advanced Composites Centre for Innovation and Science*

*Queen's Building, University Walk*

*BRISTOL BS8 1TR, UNITED KINGDOM*

*<sup>3</sup>Product Development Department, Ford OtomotivSanayi A.S.,*

*41470 Gebze, Kocaeli, TURKEY*

## ABSTRACT

A three-step Finite Element model has been implemented to predict the spring-in of L-shaped parts. The material property development during the cure has been modelled as step changes during transitions between viscous, rubbery and glassy states of the resin. The tool-part interaction is modelled as a sliding interface with a constant sliding shear stress. The effect of various material and geometric variables on the deformation of L-Section parts are investigated by a parameter sensitivity analysis. The spring-in predictions obtained by the Finite Element Method are compared to experimental measurements for unidirectional and cross-ply parts of various thicknesses and radii. Results indicate that although a 2D plane strain model can predict the spring-in measured at the symmetry plane fairly well, it is not sufficient to capture the complex deformation patterns observed.

---

<sup>1</sup>Author towhomcorrespondenceshould be made. Tel: +90 212 359 7360 E-mail: Nuri.Ersoy@boun.edu.tr

**KEYWORDS :** A. Polymer-matrix composites (PMCs), B. Residual/internal stress, C. Finite element analysis (FEA), E. Autoclave

## **I. INTRODUCTION**

Composite materials are widely used in the aerospace, marine and wind energy sectors where increasingly large structures are being designed and manufactured using composite materials and manufacturing deformations are becoming a major concern. Considerable research has been dedicated to understand the nature of these deformations and to develop models that predict these deformations in order to make necessary tool corrections [1-9]. Studies on manufacturing deformations identified various sources as intrinsic (anisotropic thermal contraction and resin shrinkage) and extrinsic (tool-part interaction). Recent studies [9-16] emphasize the effect of tool-part interaction which is a particularly significant mechanism for large parts.

Manufacturing deformations are particularly pronounced at corner sections. Corner sections usually come out with a smaller angle than the corresponding angle of the mould and this phenomenon is called spring-in. The anisotropic nature of the thermal contraction of composites causes closing of the corner sections. The deformation resulting from the thermal contraction is reversible and well understood. When the thermally contracted part is reheated to its previous temperature it takes its original shape. Anisotropic curing shrinkage has a similar effect to thermal contraction, however, it is irreversible because the shape changed is permanent when the chemical network of thermoset polymers is formed during curing. Cure shrinkage takes place at the early stages of curing when the resin still has a low shear modulus and allows the fibre stress developed at the inner surface of the corner section to be reduced due to shear deformation as shown in Figure 1(a and b).

When the laminate is laid up on a tool that has a considerably higher CTE and consolidation pressure is applied, a shear interaction develops at the tool-part interface during the temperature ramps of the Manufacturer's Recommended Cure Cycle (MRCC), putting the tows close to the tool surface in tension. This occurs at the early stages of the cure, before the resin cures, when

the resin modulus is low, resulting in a decay of tensile stresses away from the tool surface. This stress profile is locked in as the cure completes and when the part is removed from the tool, the locked in stresses cause a bending moment, forcing the part to spring out (Fig. 1.a and c).

Tool-part interaction is also included in many process models as a major contributor to the final shape of the parts [4-6]. In these models, tool-part interaction is either modelled by perfect contact with no relative motion [4], or as a cure hardening elastic shear layer which remains intact until the tool is removed [5,6,12,15,16]. By adjusting the properties of this shear layer, the amount of stress transferred between the tool and the part can be tailored. With the use of experimental data the shear layer properties are calibrated to an appropriate value. These simulations are based on semi-empirical models, which need to be calibrated according to geometrical deformations observed in manufactured parts.

In this study a finite element procedure developed previously [17] has been extended to include tool-part interaction in predicting the manufacturing distortions of corner sections, and the predictions are compared to experimental results. The previous finite element method captured the most essential mechanisms taking place during the processing of fibre reinforced thermosetting composites, like thermal contraction, cure shrinkage, and the rubbery to glassy transition. However, the tool-part interaction was left out for the sake of simplicity, and model verification was done on C-Sections manufactured in composite tooling made of the same material to minimize tool-part interaction due to differential thermal expansion of the part and the tool. In the light of recent research on the nature of tool-part interaction [18] its effect is now modelled in a more realistic way in this study as a sliding interface, using the measured tool-part interaction stresses, in contrast to previous modelling work (4-6,12-16) which depends on various assumptions about the interface behaviour.

## **2-EXPERIMENTAL WORK**

### **2.1 Material and manufacturing**

The L-shaped parts were made in a U-shaped steel tool made of IMPAX P20 Hot Work tool steel with a thermal expansion coefficient of  $12.6 \mu\text{m}/\text{m}\cdot^\circ\text{C}$ . The shape and dimensions of the tool are shown in Figure 2.a. The tool had two corners of radii 25 and 15 mm. The tool can be converted to a mini autoclave by mounting sealed top and side plates (Figure 2.b). Heat was applied through the flanges and the web of the tool with plate heaters. Pressure was applied through the compression port and vacuum can be applied through the vacuum port as represented in Figure 2.b.

The material used was a unidirectional carbon-epoxy prepreg material produced by Hexcel Composites with a designation of AS4/8552. The nominal thickness of the single prepreg was specified as 0.184 mm and the nominal fibre volume fraction as 57.4%. The physical properties of the prepreg used are given in Table 1 [19].

The manufacturer's Recommended Cure Cycle (MRCC) includes five steps. In the first step, the part is heated up to  $120^\circ\text{C}$  at  $2^\circ\text{C}/\text{min}$ . In the second step, it is held at  $120^\circ\text{C}$  for 60 minutes. In the following step, it is heated up from  $120^\circ\text{C}$  to  $180^\circ\text{C}$  at  $2^\circ\text{C}/\text{min}$ . Then, the part is held at  $180^\circ\text{C}$  for 120 minutes. Finally, the part is left to cool down to room temperature before removal from the mould. 0.7 MPa pressure is applied from the beginning to the end of the process and vacuum is applied up to the middle of the second step.

The schematic representation of the vacuum bagging is shown in Figure 3. Teflon coated glass fabric release film with a thickness of 0.08 mm was applied over the entire surface of the tool, which allows easy removal of cured parts and good slip of the prepreg on the tool. Each ply was carefully laid-up on only one side of the mould to form an L-shaped stack. The length of the mould is taken as  $0^\circ$ , and the direction running from one arm to the other across the corner is identified as  $90^\circ$  as shown in Figure 2. Vacuum of approximately -0.9bar was applied after laying every six plies to debulk the samples, to remove entrapped air and to minimize the possible effect of corner bridging. The stack was then covered with a peel ply and a breather fabric before applying a vacuum bag with the help of a sealant tape. Finally, the top and side plates of the

mould were mounted and the MRCC process was started. After processing, the mould was left to cool down to ambient temperature before the composite part was debagged and removed from the mould. A total of 20 unidirectional (UD) and cross ply (XP) specimens of various thicknesses (4, 8, 12, and 16 plies) were manufactured.

## **2.2 Measurement of Part Geometry**

The parts manufactured were scanned by a METRIS MCA II 7- axis laser scanner in order to capture the full deformation pattern of the parts. The scanned geometry of the part was virtually placed on the nominal tool through three edge points and the gap distances between the tool and the part are obtained at discrete points over the surface. In order to calculate spring in values, gap distances were read on both flanges, at five equally spaced points along 5 stations, as represented in Figure 4. The spring-in angle was measured by drawing secant lines on the arms.

For thickness measurement, both sides (tool and bag side) of the laminates were scanned. In order to reveal the effect of corner thickening, thickness measurement was performed along the length of the laminates at seven stations along the length.

## **3- FINITE ELEMENT ANALYSIS**

A three step 2-D finite element model including anisotropy in the thermal expansion coefficient, cure shrinkage, consolidation, and tool-part interaction was developed to predict the process induced stresses and deformation. The basic process model was developed and implemented in ABAQUS previously by Ersoy et al [17]. The three steps of the model represent the viscous, rubbery, and glassy states of the resin. The reason for preferring a three step approach is the complexity of determining continuous development of material properties during the cure cycle. The constitutive equations are based on the Cure Hardening Instantaneously Linear Elastic model previously proposed by Svanberg and Holmberg [20]. In each step constant material properties were used. The two main transitions during the curing process are gelation, occurring

at approximately 30 % degree of conversion, and vitrification, occurring at approximately 70 % degree of conversion of the resin[17].

### **3.1 Steps of analysis**

The resin states with respect to the MRCC is shown in Figure 5 together with the glass transition temperature of the resin. The gel point which is defined as the point where the prepreg is cured enough to sustain in-plane shear stresses, and the vitrification point at which the instantaneous glass transition temperature reaches the process temperature are also indicated. The resin is believed to be gelled at around 160 degrees during the second ramp as a sharp rise of the glass transition temperature. The vitrification occurs 45 mins. After the 180 °C soak period starts [21].

In the first step of the model, before gelation, the composite is in the viscous state and assumed not to sustain any mechanical stress in the transverse direction, whereas it can sustain some fibre stresses due to fibre friction. Consolidation takes place as the voids are suppressed, expelled from the composite, and extra resin bleeds out in this step. Due to the difficulty in measuring the mechanical properties in the viscous state, there is no reliable data available for this state in the literature. In order to investigate the effect of the shear modulus in the viscous state, a parametric study is carried out by taking the shear modulus as different fractions of the rubbery shear modulus.

In the second step, between gelation and vitrification, rubbery material properties were used. Due to cross-linking reactions, cure shrinkage takes place during the curing of thermosetting resins, which results in contraction in the through thickness direction.

In the last step, after vitrification, glassy material properties were used in the model. The resin vitrifies and transforms to the glassy state and the resin modulus increases to a magnitude of a few GPa. The stresses developed in the viscous and rubbery states are rearranged as the part is allowed to deform freely as it cools down to room temperature by removing the boundary conditions.

The properties of AS4/8552 composite in the rubbery and glassy states were found in previous work [21] and are shown in Table 2. Cure shrinkage and CTE of the composite in the fibre direction assumed to be zero in Table 2. Gelation occurs when the temperature reaches to 160°C during the second ramp and vitrification occurs at 45 min after the start of the second hold at 180°C [17,21]. The CTE value given in this table for glassy state is the nominal value, and actual values are calculated as a function of corner thickness. To obtain the experimentally measured 0.48% [22] transverse cure shrinkage in the rubbery state, an equivalent negative coefficient of thermal contraction is used as given in Table 2. In Step-1 and Step-2, an autoclave pressure of 0.7 MPa is applied on the bag surface of the part. In Step-3, the applied pressure is removed, the part is separated from the tool and spring-in and warpage develop. A uniform temperature was assigned to the parts because the temperature range measured across the thickness and in the plane of the part at eight stations was within a 3 °C band for even the thickest (16 plies) laminates.

### **3.2 Implementation of mechanical properties**

The mechanical properties in each step are different, so these properties are implemented in the analysis by means of a user subroutine UMAT, which updates the elastic properties at the beginning of each step, and the stresses locked-in at each step are added up to find the final stress state after removal from the mould. The reader should refer to Ref [17] for details of the implementation of the UMAT subroutine in the analysis.

### **3.3 Tool-part interaction**

Tool part interaction is examined in detail by Gartska et al. [18] by means of an instrumented ply technique with the same material. They found that when the resin is in the viscous state, the tool-part interaction is basically due to fibre friction, and a sliding friction with a constant shear stress of 0.1 MPa prevails. However, once the resin gels, the nature of the interaction changes to a stick-slip type, resulting in a stable state with a constant shear stress of 0.2 MPa at the interface. In the present study, although the tool material and the interface properties are different, constant

shear stress of 0.1 MPa and 0.2 MPa are used for viscous and rubbery steps respectively as a reference, since the interfacial stress has not been measured directly, and the effect of varying them is investigated.

Interaction between tool and part is modelled by using ABAQUS mechanical contact interaction modelling capabilities [23]. In the model, contact surfaces are defined for interactions, using the ABAQUS option \*SURFACE, and then these surfaces are matched by using the option \*CONTACT PAIR. The characteristic of the contacting surfaces are defined by using the option \*SURFACE BEHAVIOUR. Interaction normal to the surface is the default “hard” contact relationship, which allows no penetration of the slave nodes into the master surface and no transfer of tensile stress across the interface. Interaction tangential to the surface is modelled by the classical isotropic Coulomb friction model. The interfacial shear stress is assumed proportional to the contact pressure up to a limiting sliding stress. The constant of proportionality is the friction coefficient,  $\mu$  and the sliding stress is  $\tau_{\max}$ .

In the first and the second step of the analysis tool-part interaction is active and in the third step tool-part contact is deactivated. Following the findings of Garstka et al. [18], the sliding stress  $\tau_{\max}$  is changed from 0.1 MPa to 0.2 MPa in the second step because the friction behaviours of these two steps (viscous and rubbery) are different.

### **3.4 Meshing and boundary conditions**

The L-section-composite parts of 100 mm arm length and 15 and 25 mm corner radius were modelled together with the female steel tool, as shown in Figure 6. Only half of the part is modelled by taking advantage of the symmetry condition. A local coordinate system is used so that the 2-axis is aligned with the surface of the tool. The elastic modulus of the tool material was taken to be 200 GPa and thermal expansion coefficient to be  $12.6 \times 10^{-6} \text{C}^{-1}$ .

The elements used in the code are 8-node biquadratic quadrilateral generalized plane strain elements with reduced integration. Aspect ratio of the elements is 5.4 and 3.8 for laminate’s flat and curve section respectively and it is 2.7 for tooling part. The name of the element in

ABAQUS is CPEG8R [23]. The generalized plane strain theory used in ABAQUS assumes that the model lies between two planes that can move with respect to each other. It is assumed that the deformation of the model is independent of position with respect to axial direction. The relative motion of the two planes results in a direct strain in the direction perpendicular to the plane of the model only. The defined generalized plane strain elements have an extra node with 3 degrees of freedom; an out-of-plane translation and two rotations. Restraining this node gives a plane strain condition, whereas releasing the node gives no overall stress in the out-of plane direction[23]. In the model, two reference nodes are defined, for the tool and the part, in all the steps for unidirectional parts. These reference nodes are coupled and restrained for rotation in the first and second steps so that the two bounding planes displace with respect to each other but do not rotate, which allows the thermal expansion effect of the tool perpendicular to the plane of the model to be considered, and such restraint prevents the spread of the part on the tool under pressure in the first and second steps. In cross-ply parts, only one reference node is defined, since the fibres perpendicular to the plane restrain the part from spreading on the tool. In Step-3, removal of the part from the tool is simulated by removing the FE model for tool by the help of \*MODEL CHANGE option of ABAQUS, so that the part is now in an overall plane stress condition; the absence of external forces in Step-3 validates this condition. However, in the cross-ply laminates, there are still stresses in the out of plane direction due to the mismatch in CTE values of individual plies in this direction.

The sliding boundary conditions on the flat upper side of the tool enable the tool to expand or contract along the longitudinal direction but prevent free body motion of the tool. On the symmetry line, symmetry boundary conditions are used. Autoclave pressure is applied at the lower side of the laminate as a surface pressure.

#### **4. RESULTS AND DISCUSSION**

In the experimental study, the free variables are the stacking sequence (cross-ply and unidirectional), laminate thickness (4, 8, 12 and 16 plies), and the corner radius (15 mm and 25

mm), and the effect of these variables on the spring-in is investigated. Examples for the designation of the specimens are as follows: 8UD-R15 corresponds to a unidirectional 8-ply thick,  $[90]_8$  L-section with 15 mm corner radius with fibres running from one arm to the other across the corner. Similarly 16XP-R25 corresponds to a 16-ply crossly  $[90/0]_{4s}$  L-section with 25 mm corner radius. The effect of corner radius, thickness, composite mechanical properties and friction properties on the spring-in values in the viscous and rubbery state is considered in a parameter sensitivity analysis.

#### 4.1 Parameter sensitivity analysis

Although there are certain values available for the elastic and shear moduli in the rubbery state ( $E_{22}^{rub}$ ,  $G_{12}^{rub}$ ) it is not easy to measure or estimate the corresponding pseudo-elastic moduli values in the viscous state ( $E_{22}^{vis}$ ,  $G_{12}^{vis}$ ). In order to assess the effects of the various geometric and material parameters on spring-in, a parametric study was conducted using the FEA model. The parameters investigated are: stacking sequence, corner radius, number of plies, transverse and shear moduli in the viscous and rubbery states,  $E_{22}^{vis}$ ,  $G_{12}^{vis}$ ,  $E_{22}^{rub}$ ,  $G_{12}^{rub}$ , friction coefficient and sliding stress in viscous and rubbery states,  $\mu^{vis}$ ,  $\tau_{max}^{vis}$ ,  $\mu^{rub}$ , and  $\tau_{max}^{rub}$ . Factors and their values are summarized in Table 3. In total, 32 parameter study runs were solved by FEA. The percent effects for spring-in are shown in Figures 7. It is seen that the stacking sequence, number of plies,  $\tau_{max}^{vis}$ ,  $E_{22}^{vis}$ , and  $G_{12}^{vis}$  are the most important parameters for the spring-in.

#### 4.2 Corner thickening.

The corner thickening for 16-ply thick parts can be seen easily from the thickness measurement along the length of the laminates in Figure 8. This figure shows the thickness at the mid-section normalized by the nominal thickness along the part. It can be seen clearly that the resin at regions close to the corner has percolated into the corner, resulting in an increase in thickness of the corners above the nominal value. This phenomenon has also been observed by Hubert and Poursartip [24]. The parts with 15 mm radius have greater corner thickening compared to the

parts with 25 mm radius and unidirectional parts have greater corner thickening compared to cross-ply parts. The resin flow is lower in cross-ply parts compared to unidirectional parts.

Since the thermo elastic component of spring-in is determined by through-the-thickness CTE during the cooling step of the model developed to predict the spring-in, fibre volume fractions and the CTEs are calculated at the corner for each specimen. The corner fibre volume fraction is found from the deviation from the nominal thickness of the part and nominal fibre volume fraction (given in Table 1) supplied by the manufacturer [19].

The coefficient of thermal expansion is calculated at the corner for each specimen separately by using the following expression which is based on Self Consistent Micromechanics Theory [25]:

$$\alpha_2 = (\alpha_{f2} + \nu_{f12}\alpha_{f1})V_f + (\alpha_r + \nu_r\alpha_r)(1-V_f) - [\nu_{f13}V_f + \nu_r(1-V_f)] \left[ \frac{\alpha_{f1}E_{f11}V_f + \alpha_rE_r(1-V_f)}{E_{f11}V_f + E_r(1-V_f)} \right] \quad (1)$$

where  $\alpha_{f1}$  and  $\alpha_{f2}$  are longitudinal and transverse CTE of the fibre respectively,  $\alpha_r$  is the CTE of the resin,  $\nu_{f12} = \nu_{f13}$  are fibre Poisson ratios,  $\nu_r$  is the resin Poisson ratio,  $E_{f11}$  is the longitudinal fibre elastic modulus,  $E_r$  resin elastic modulus, and  $V_f$  is the fibre volume fraction.

### 4.3 Thermoelastic spring-in

In order to distinguish the contributions of thermoelastic (thermal contraction), and non-thermoelastic (cure shrinkage, and tool part interaction) factors on spring in, a study was carried out and the results are shown in Figures 9-12. To show the effect of anisotropic thermal contraction, only the third (cool-down) step is run, with glassy state material properties, and calculated CTEs which alter from the nominal value due to corner thickening. Corner thickening results in a higher resin fraction, and higher through-the thickness CTEs. The effect of thermal contraction on spring-in does not change significantly by corner thickening, as shown by the approximately constant values of thermoelastic contraction for the different thickness cases with different degrees of corner thickening in Figures 9-12. Highest corner thickening takes place in the thickest unidirectional specimen with the smallest radius, namely UD16-R15 (Figure11), and this increases the thermoelastic contribution from 0.37 to 0.43 degrees.

#### 4.4. Effect of sliding stress and viscous state shear modulus.

In the finite element model, the curing of the composite was modelled as step transitions between the viscous, rubbery, and glassy states. The material properties in the rubbery and glassy states were determined with proper experimental or analytical methods [21], however the nature of the material during the viscous state is rather difficult to assess. The resin is in a viscous state, and it is assumed not to carry any stress, however it has been observed that considerable fibre stress may develop in the early stages of cure due to fibre friction within the plies and at the tool-part interface [9, 18]. This observation suggests that the tool-part interaction stress is transferred through the thickness of the material to a certain extent, and the material should exhibit a certain shear modulus. This property is difficult to measure, and a parametric study was carried out in this study to assess the effect of the interface shear stress and shear modulus of the material in the viscous state. For this reason, the interface sliding shear stress is varied between  $\tau_{\max} = 0.10$ , 0.15, and 0.20MPa. These are typical values for the AS4/8552-Al tool system [9, 18]. The viscous shear modulus of the composite is taken to be either the full rubbery modulus  $(G_{12}^{rub}, G_{23}^{rub})$  or one-tenth of the rubbery modulus  $(G_{12}^{rub}/10, G_{23}^{rub}/10)$ . In Figures 9-12, predicted spring-in values are plotted together with the experimental values as a function of thickness. Due to the warpage in the 3<sup>rd</sup> direction (perpendicular to the plane of the 2-D model) the spring in values are not constant along the length of the specimens. The experimentally observed deformation pattern is schematically shown in the small inset in Figure 10. Hence corresponding values at the mid-section (unfilled diamonds), as well as the values at other stations (filled diamonds) are plotted on the same graph. It can be seen that the effect of the viscous shear modulus is more dominant than the interface sliding shear stress, and if the viscous shear modulus is high, increasing the interface sliding shear stress has a smaller effect on the predicted spring-in values. It can also be observed that closer predictions are obtained with the lower viscous shear modulus. Another observation can be made regarding the trend of predicted spring-

in values with thickness. In order to explain this observation one should keep in mind that spring in is a result of counteracting mechanisms: consolidation and cure shrinkage in the early stages of cure results in tensile stresses on the bag side fibres resulting in spring-in and tool part-interaction on the tool side resulting in spring-out. The observed net effect of these mechanisms depends on their relative magnitudes as well as the thickness of the part, since as the thickness increases; stiffness of the part also increases reducing deformation due to residual stresses. This explains why the spring-in angle reduces with increasing thickness. When the viscous shear modulus is taken to be equal to rubbery shear modulus, ( $G^{vis} = G^{rub}$ ), the effect of tool part interaction is minimal due to shear lag along the thickness. However, if the viscous shear modulus is sufficiently low as compared to rubbery shear modulus, ( $G^{vis} = G^{rub} / 10$ ), the fibre stress gradient due to tool-part interaction is effective, resulting in a lower spring-out in thinner specimens with a lower bending stiffness. Lower viscous shear modulus increases the relative effect of the tool-part interaction in the overall spring-in value, and reverses the trend observed in spring-in with increasing thickness.

It can be seen clearly that thinner specimens have more variation in spring-in values, showing the obvious non constant nature of the spring in along the length of the specimens due to warpage in the 3<sup>rd</sup> direction (axial, or perpendicular to the model plane). This effect is expected to be less prominent for thicker specimens, giving less scatter in the spring-in measurements in Figures 9-12.

This can be explained by the fact that tool-part interaction along the 3<sup>rd</sup> direction (axial, or perpendicular to the model plane) is less effective than in the 2<sup>nd</sup> direction for UD parts due to easy deformation of the very compliant resin along the 3<sup>rd</sup> direction during the viscous and rubbery states, hence warpage due to tool-part interaction along the 3<sup>rd</sup> direction is low for UD parts. On the other hand for XP parts, fibres along the 3<sup>rd</sup> direction constrain the composite against expansion of the tool, so that tool-part interaction is more effective along the 3<sup>rd</sup> direction and causes more warpage as can be seen in Figure 13.

In addition to tool-part interaction along the 3<sup>rd</sup> direction, varying consolidation can be another reason for non-constant spring-in along length direction. A different deformation pattern and more scatter in spring-in values were observed in the UD16-R15 case in Figure 11. For this specimen, the spring in value at the mid-section is lower than at the edge sections. This observation can be explained by referring to the thickness measurement along the 3<sup>rd</sup> direction at the corner (4<sup>th</sup> station in Figure 8). The thickness of the mid-section at the 4<sup>th</sup> station is higher as compared to the thickness of the edges at the 4<sup>th</sup> station. The higher consolidation at the edges results in higher fibre stresses at the bag side towards the edges. These residual stresses cause the part to bend inward along the 3<sup>rd</sup> direction so that spring-in values at the edges will become higher than at the mid-section compared with the other specimens

#### **4.5 Stresses developed during curing**

Figure 14 shows the numerical results for the fibre direction stress distribution through the thickness taken from the FE Model solution for the UD4-R15 part at the end of the second and third step. Here the stresses are calculated according to the local coordinate system shown in Figure 6. It can be seen that the fibre direction stress,  $\sigma_{22}$ , increases towards the corner of the part. It has been observed that during the 1<sup>st</sup> and 2<sup>nd</sup> Steps tensile stresses are developing at the corner in the bag and tool side. Consolidation and cure shrinkage taking place during the 1<sup>st</sup> and 2<sup>nd</sup> Steps causes stretching of the fibres on the bag side. Tool-part interaction causes stretching of the fibres on the tool side. The resulting stress distribution is tensile along the thickness direction, with higher tensile stresses on the tool and bag side. The stresses are rearranged to give a residual stress distribution at the end of third step.

As can be seen from Figure 15 which shows the  $\sigma_{22}$  values for the cross-ply samples, which exhibits a zig-zag pattern and a curvilinear distribution superimposed together. The zig-zag distribution is the typical self-balancing residual stress pattern that can be observed in cross-ply laminates during cooling from processing temperature, whereas the curvilinear stress distribution

similar to the unidirectional parts is due to the combined effect of consolidation, cure shrinkage, and tool-part interaction.

Another observation is the fact that fibre direction stresses on the bag side at the end of the second step are higher in the cross-ply compared to the unidirectional parts. This is basically due to higher cure shrinkage in XP parts due to the constraints imposed by the fibres in the two planar directions. This observation, in addition to the fact that the cross-ply samples have less bending stiffness explains why the cross-ply parts give more spring-in than the unidirectional ones.

#### **4.6 Tool-part interaction**

As seen in Figure 16, the finite element analysis showed that opening of the contact interface occurs at the corner of the L-shaped parts, which results from cure shrinkage in the second step of the model and fibre bridging of the corner. Experimental results confirm this opening by corner thickening and the poor surface finish of the corner as seen in Figure 17. In Figure 18 the autoclave pressure, frictional shear stress, separation from the tool, and relative displacement between the tool and the part are shown at the end of step 2 for the UD16-R25 part. The autoclave pressure is ineffective at the corner of the part due to fibre bridging, which causes the part to disengage from the tool at the corner. The opened region at the corner is percolated by resin so that the thickness of the part at the corner increases and a resin rich layer is formed at the surface. The corner thickness of the parts with 15 mm radius is greater than the parts with 25 mm radius so that cure shrinkage is higher in the former parts. It can also be seen from Figure 18 that slipping with constant shear stress prevails for most of the interface on the arms.

### **5. CONCLUSIONS**

A finite element method previously developed is extended successfully to account for the effect of tool-part interaction on the prediction of spring-in angles of unidirectional and cross-ply L-shaped parts of various thicknesses. The tool-part interaction is modelled as a sticking-sliding interface using contact elements. The modelling work and the observations cast more light on the

nature of tool-part interaction during composites manufacturing. It is observed that stresses developed due to tool-part interaction may cause separation of the part from the tool during manufacturing. The spring-in predictions and experimental data are compared and the reasons for the discrepancies between the two are discussed. It has been found that the effective shear modulus of the composite early in the cure has a more pronounced effect on predicted spring-in compared to the interface sliding stress. It has been observed that the three step 2-D model captures most features of the geometry development at the corner sections, except the deformation in the direction perpendicular to the model plane due to tool-part interaction in this direction which would require a full 3-D analysis.

## **5. ACKNOWLEDGEMENTS**

Nuri Ersoy and Kenan Çınar acknowledge the support of Boğaziçi University Research Fund for and Istanbul Development Agency (ISTKA) for their support under project codes 09A601 and ISTKA/BIL/2012/58 respectively.

## **6. REFERENCES**

- [1] White SR and Hahn HT. Process modelling of composite materials: residual stress development during cure. Part II. Experimental validation. *J Compos Mater* 1992;26(16):2423–2453.
- [2] Bogetti TA and Gillespie JW. Process-induced stress and deformation in thick-section thermoset composite laminates. *J Compos Mater* 1992; 26(5):626–659.
- [3] Radford DW and Rennick T. Separating sources of manufacturing distortion in laminated composites. *J Reinforced Plast Compos* 2000;19(8):621–641.
- [4] Zhu Q, Geubelle PH, Li M and Tucker III CL. Dimensional accuracy of thermoset composites: simulation of process-induced residual stresses. *J Compos Mater* 2001; 35(24): 2171-2205.
- [5] Johnston A, Vaziri R and Poursartip A. A plane strain model for process induced

- deformation of laminated composite structures. *J Compos Mater* 2000;35(16):1435–1469.
- [6] Fernlund G, Rahman N, Courdji R, Bresslauer M, Poursartip A, Willden K and Nelson K. Experimental and numerical study of the effect of cure cycle, tool surface, aspect ratio, and the lay-up on the dimensional stability of autoclave-processed composite parts. *Composites Part A* 2002;33:341–351.
- [7] Darrow DA and Jr Smith LV. Isolating components of processing induced warpage in laminated composites. *Journal of Composite Materials* 2002; Vol. 36, No. 21
- [8] Albert C and Fernlund G. Spring-in and warpage of angled composite laminates. *Composites Science and Technology* 2002; 62: 1895–1912.
- [9] Wisnom MR, Gigliotti M, Ersoy N, Campbell M and Potter KD, Mechanisms generating residual stresses and distortion during manufacture of polymer–matrix composite structures. *Composites Part A* 2006;37:522–529
- [10] Twigg G, Poursartip A and Fernlund G. An experimental method for quantifying tool–part shear interaction during composites processing. *Composites Science and Technology* 2003; 63: 1985–2002.
- [11] Twigg G, Poursartip A, and Fernlund G, Tool-part interaction in composites processing. Part I: Experimental investigation and analytical model. *Composites Part A* 2004; 35: 121-133
- [12] Twigg G, Poursartip A and Fernlund G. Tool-part interaction in composites processing. Part II: Numerical modelling. *Composites Part A* 2004; 35: 135-141.
- [13] Ersoy N, Potter K, Wisnom MR and Clegg MJ. An experimental method to study the frictional processes during composites manufacturing. *Composites Part A* 2005; 36: 1536–1544.
- [14] Potter KD, Campbell M, Langer C and Wisnom MR. The generation of geometrical deformations due to tool/part interaction in the manufacture of composite

- components. *Composites Part A* 2005;36: 301–308.
- [15] Abdul R, Arafath A, Reza V and Anoush P. Closed-form solution for process-induced stresses and deformation of a composite part cured on a solid tool: Part I – Flat geometries, *Composites Part A* 2008; 39: 1106–1117
- [16] Abdul R, Arafath A, Reza V and Anoush P. Closed-form solution for process-induced stresses and deformation of a composite part cured on a solid tool: Part II – Curved geometries. *Composites Part A* 2009;40: 1545-1557.
- [17] Ersoy N, Garstka T, Potter K et al. Modelling of the spring-in phenomenon in curved parts made of a thermosetting composite. *Composites Part A* 2010;41: 410-418
- [18] Garstka T, Ersoy N, Potter K, and Wisnom MR. Observations of tool-part interaction in curved composite laminates, submitted to *Composites Part A*
- [19] HexPly 8552 Epoxy matrix (180°C/356°F curing matrix), Product Data, *Hexcel Composites*. Publication FTA 072c; October, 2008.
- [20] Svanberg JM, Holmberg JA. Prediction of shape distortions. Part I. FE implementation of a path dependent constitutive model. *Composites Part A* 2004;35:711–721.
- [21] Ersoy N, Garstka T, Potter K et al. Development of the properties of a carbon fibre reinforced thermosetting composite through cure. *Composites Part A* 2010; 41: 401-409
- [22] Garstka T, Ersoy N, Potter K, and Wisnom MR. In situ measurements of through-the-thickness strains during processing of AS4/8552 composite. *Composites: Part A* 2007; 38: 2517–2526
- [23] Hibbit, Karlson, and Sorensen Inc. *ABAQUS Online Documentation* 2004; Version 6.5-1.
- [24] Hubert P and Poursartip A. Aspects of the Compaction of Composite Angle Laminates: An Experimental Investigation. *J Compos Mater* 2001; 35(1):2-26
- [25] Hull D., *Introduction to Composite Materials*, Dover Publications, 1981.

**Table 1.** Physical properties of AS4/8552 [19]

	<b>Value</b>	<b>Units</b>
<b>Fibre Density</b>	1.79	g/cm <sup>3</sup>
<b>Resin Density</b>	1.30	g/cm <sup>3</sup>
<b>Nominal Cured Ply Thickness</b>	0.184	mm
<b>Nominal Fibre Volume</b>	57.42	%
<b>Nominal Laminate Density</b>	1.58	g/cm <sup>3</sup>

**Table 2.** Material properties in the rubbery and the glassy state [22].

<b>Property</b>	<b>Unit</b>	<b>Rubbery</b>	<b>Glassy</b>
$E_{11}$	MPa	132200	135000
$E_{22} = E_{33}$	MPa	165	9500
$G_{12} = G_{13}$	MPa	44.3	4900
$G_{23}$	MPa	41.6	4900
$\nu_{12} = \nu_{13}$	-	0.346	0.3
$\nu_{23}$	-	0.982	0.45
$\alpha_{11}$	$\mu\epsilon/^\circ\text{C}$	-	0*
$\alpha_{22} = \alpha_{33}$	$\mu\epsilon/^\circ\text{C}$	-31.7	32.6
$\epsilon_{11}^{cure}$	%	0*	-
$\epsilon_{22}^{cure} = \epsilon_{33}^{cure}$	%	0.48	-

\*Assumed to be zero

**Table 3.**Factor values used in parameter study.

Factors	Baseline	Values			
Radius (mm)	15	15	25		
Number of plies	4	4	8	12	16
$E_{22}^{vis}$ (MPa)	80	64	80	96	
$G_{13}^{vis}$ (MPa)	20	16	20	24	
$E_{22}^{rub}$ (MPa)	165	132	165	198	
$G_{12}^{rub}$ (MPa)	44.3	35.4	44.3	53.1	
$\tau_{max}^{vis}$ (MPa)	0.10	0.08	0.10	0.12	
$\mu_{max}^{vis}$	0.30	0.24	0.30	0.36	
$\tau_{max}^{rub}$ (MPa)	0.20	0.16	0.20	0.24	
$\mu_{max}^{rub}$	0.30	0.24	0.30	0.36	

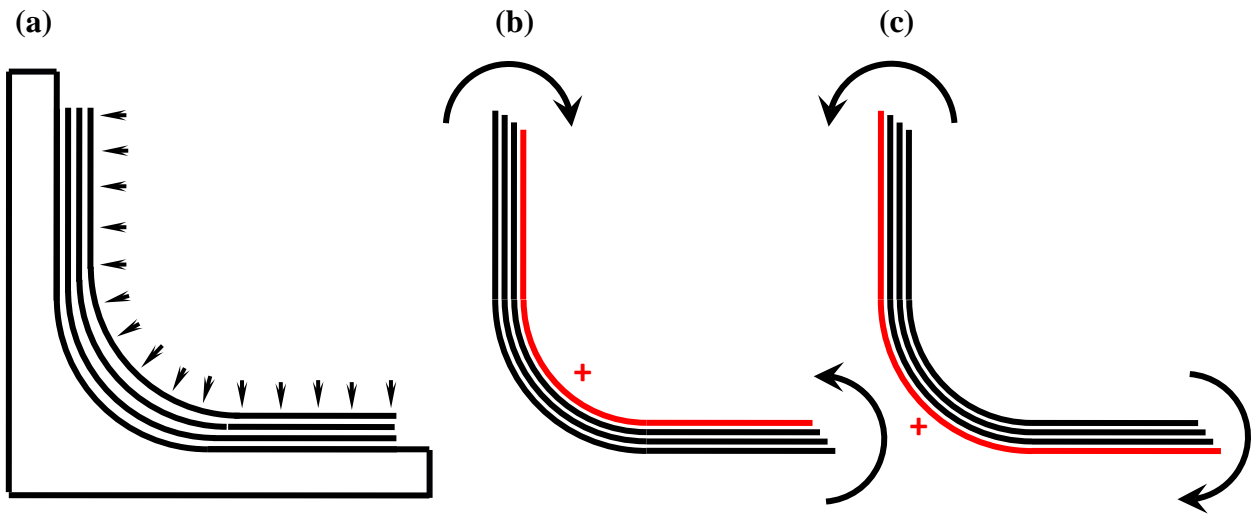


**Figure 1.** (a) Manufacturing of a corner section in female tool (b) effect of cure shrinkage (c) effect of tool-part interaction

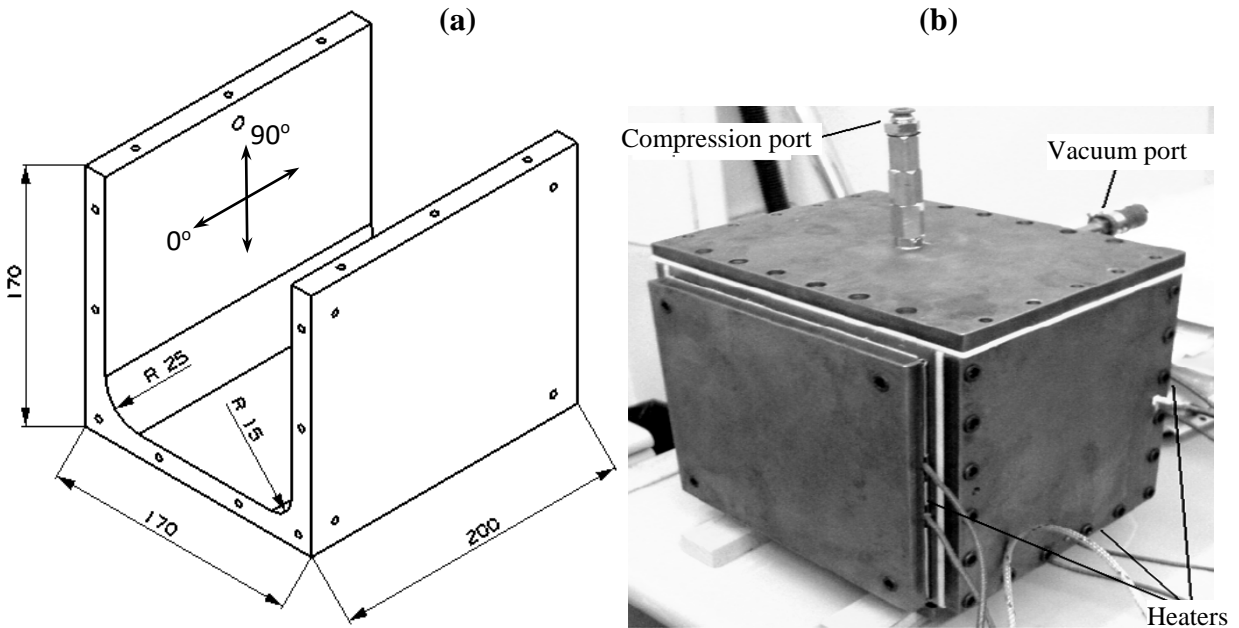


**Figure 2.** The mould used in manufacturing: (a) dimensions in mm. (b) closed to form an autoclave

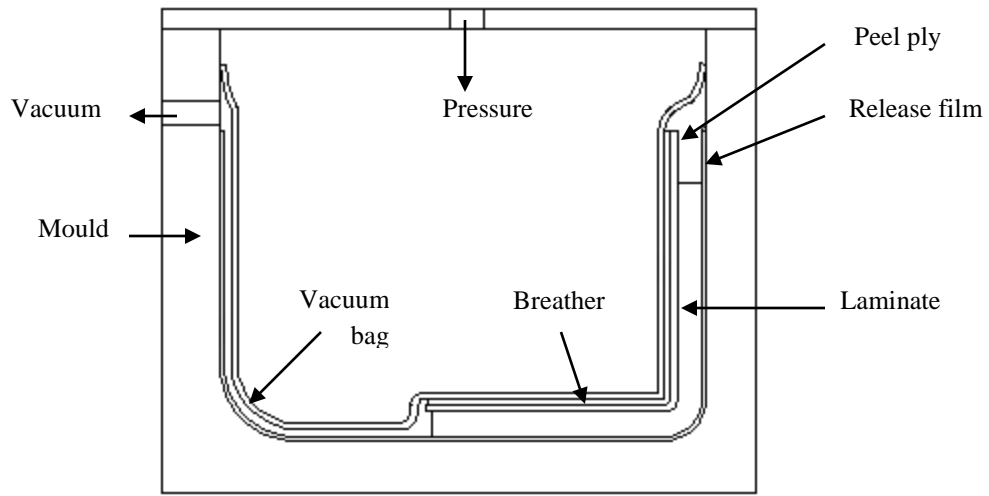


**Figure 3.** Schematic representation of specimen fabrication.

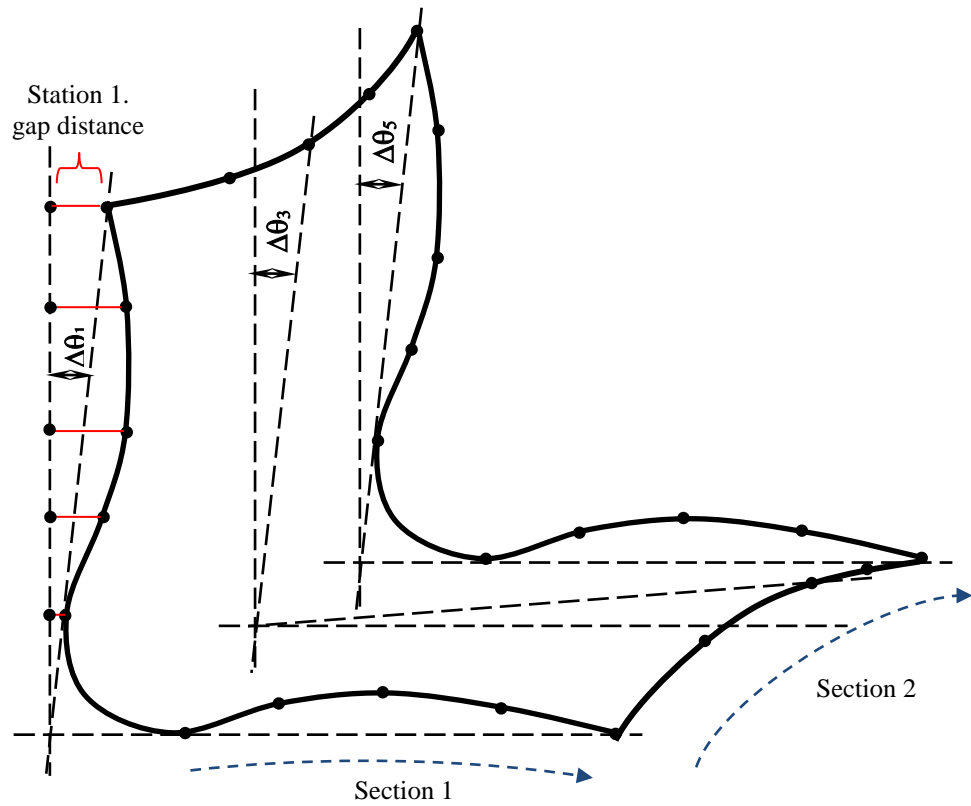


**Figure 4.** Measurement of the spring-in angle

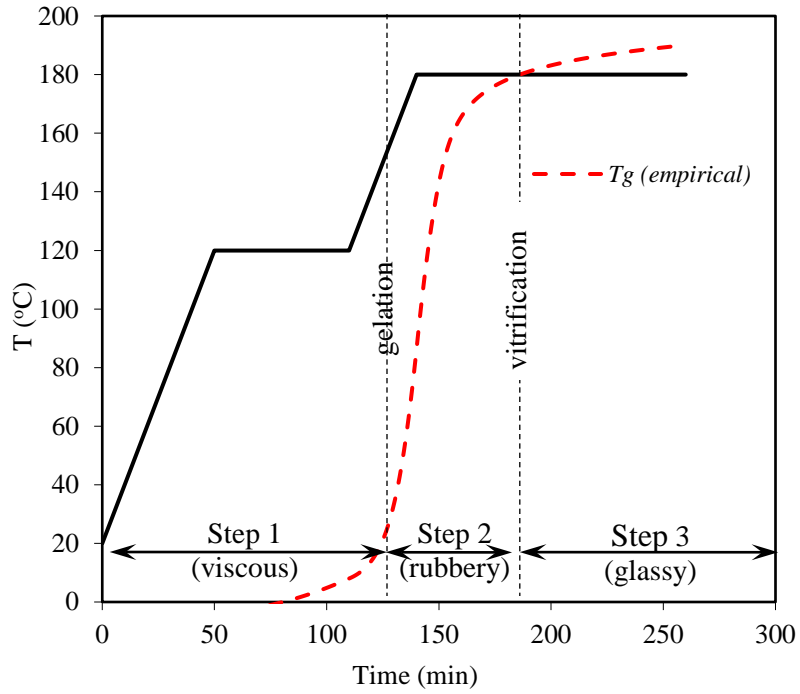


**Figure 5.** Various stages of the MRCC

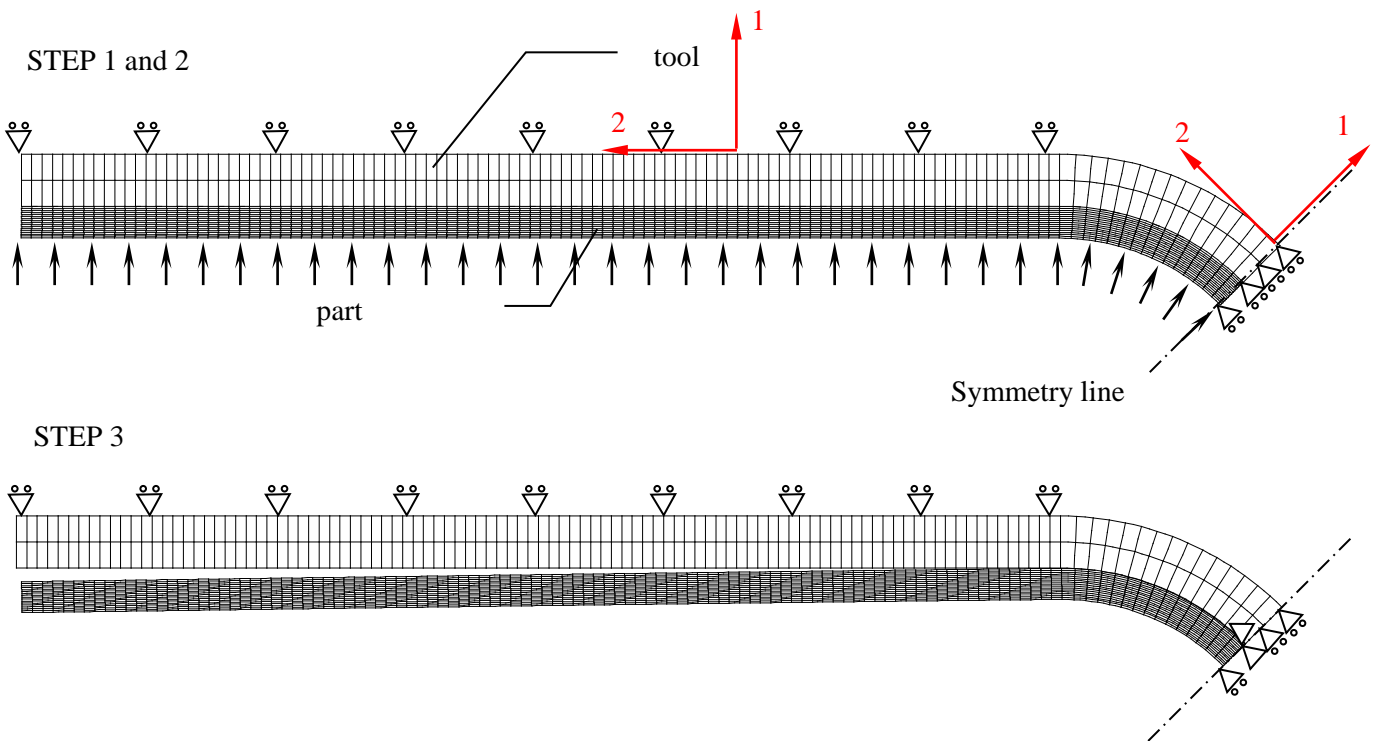


**Figure 6.** The Finite Element mesh and boundary conditions at steps 1, 2 and 3.

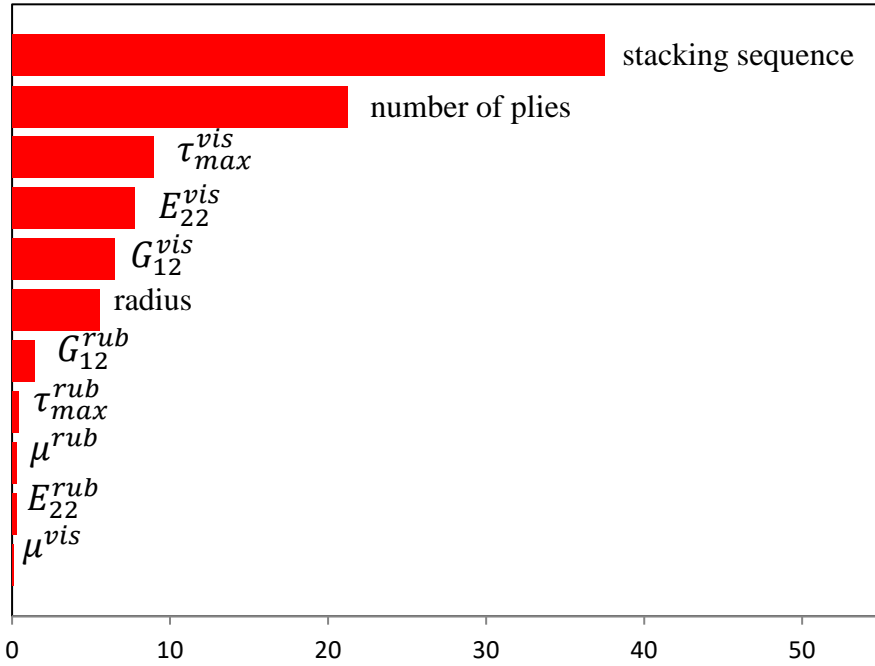


Figure 7. Percent effect on spring-in of the DOE factors.

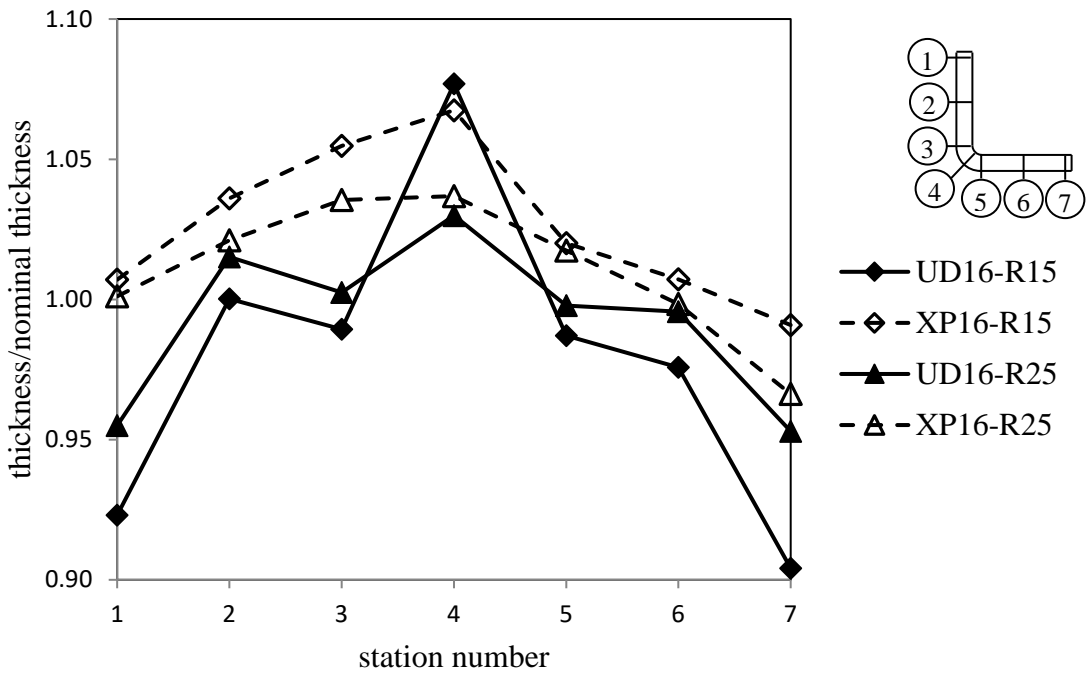
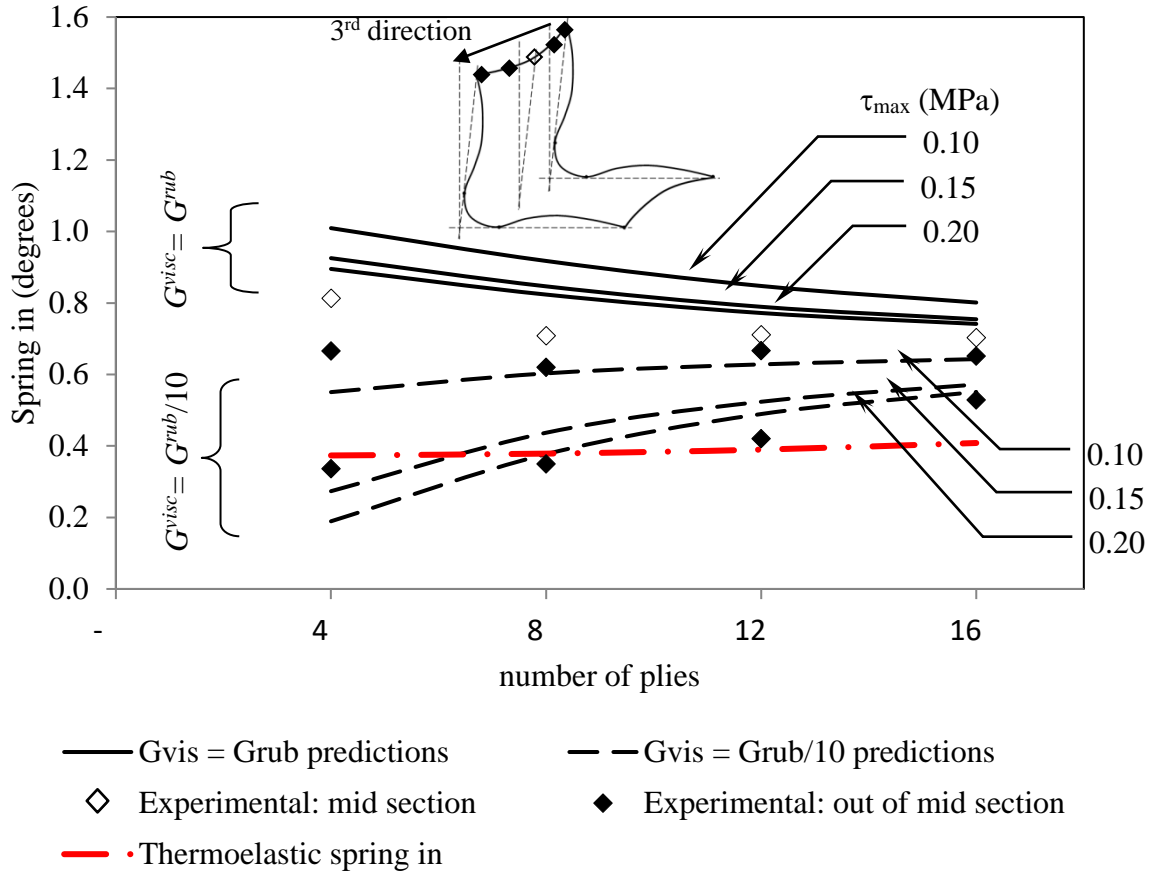
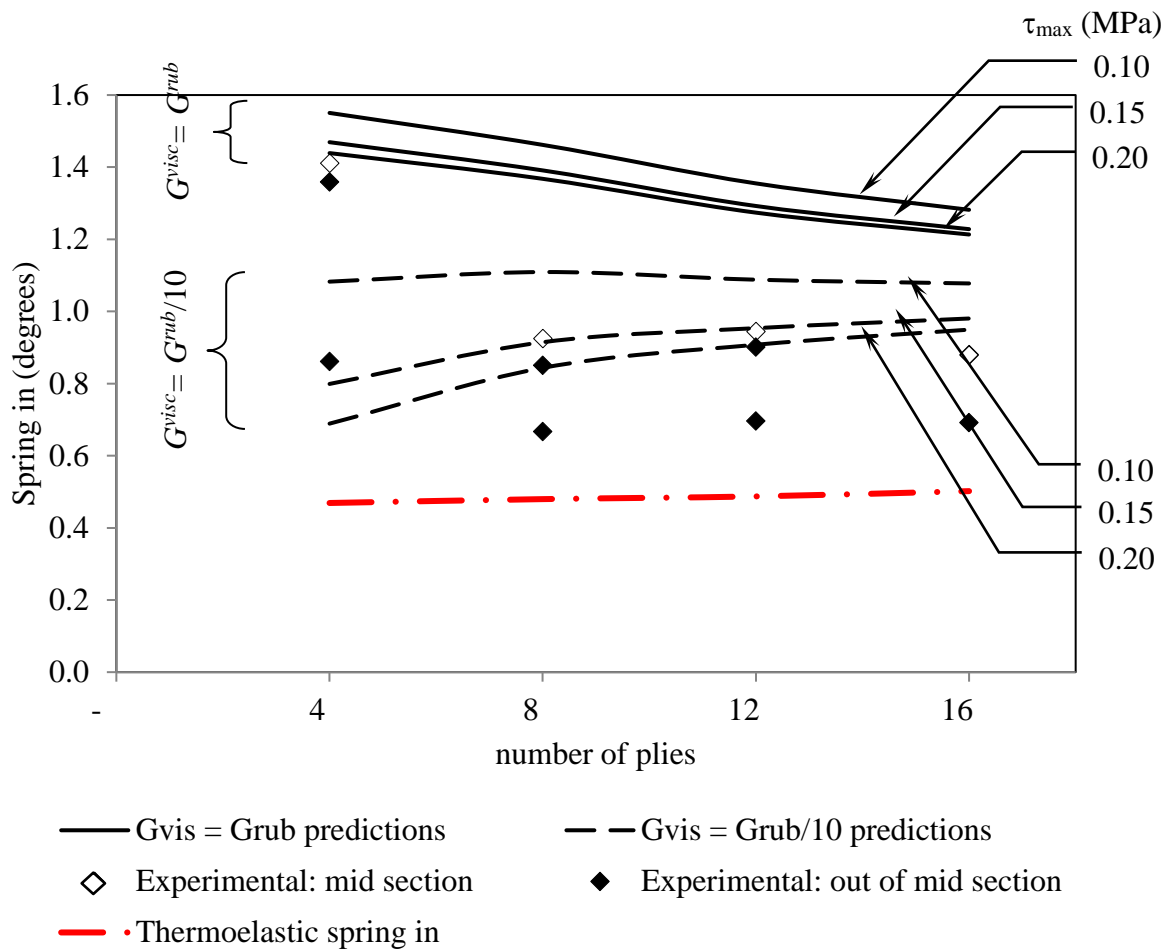


Figure 8. Corner thickening effect.



**Figure 9.**Effect of sliding shear stress and viscous shear modulus on spring-in predictions for UD-R25 parts.



**Figure 10.** Effect of sliding shear stress and viscous shear modulus on spring-in predictions for XP-R25 parts.

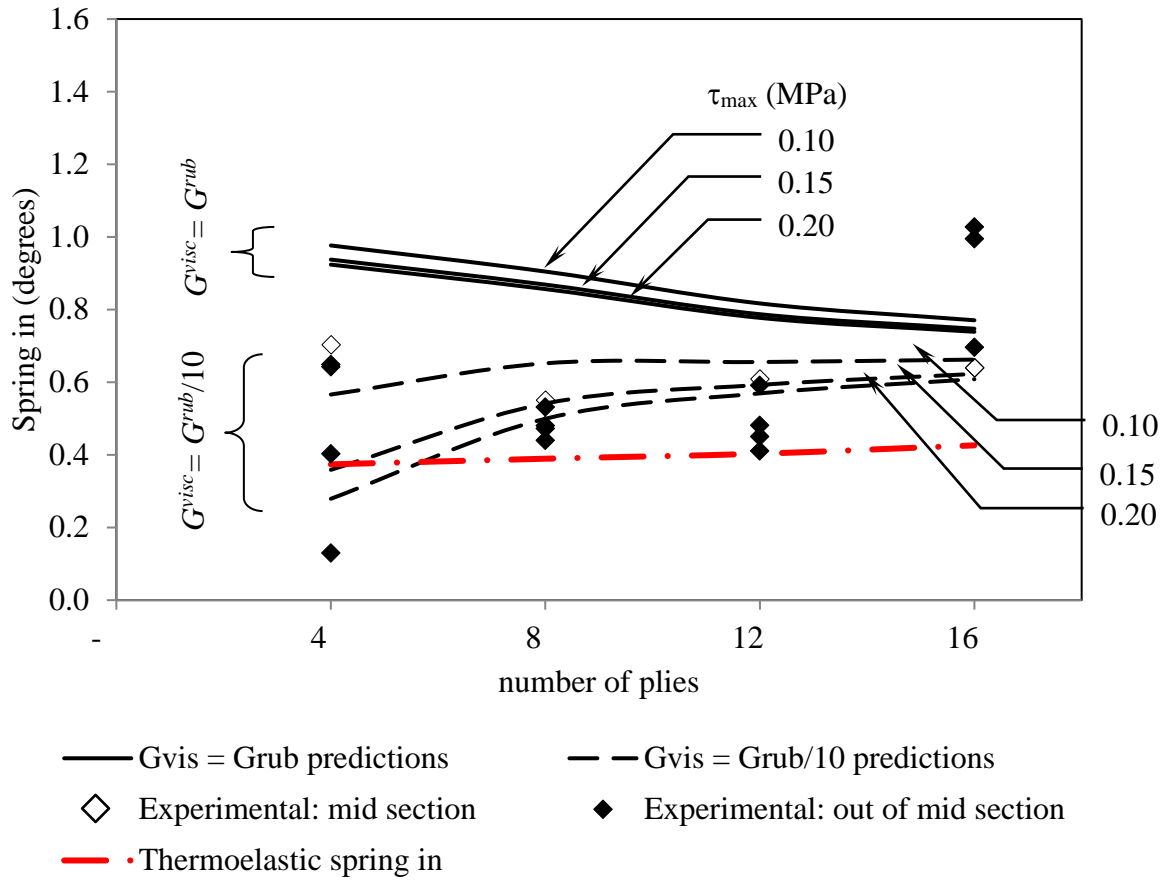


**Figure 11.** Effect of sliding shear stress and viscous shear modulus on spring-in predictions for UD-R15 parts.

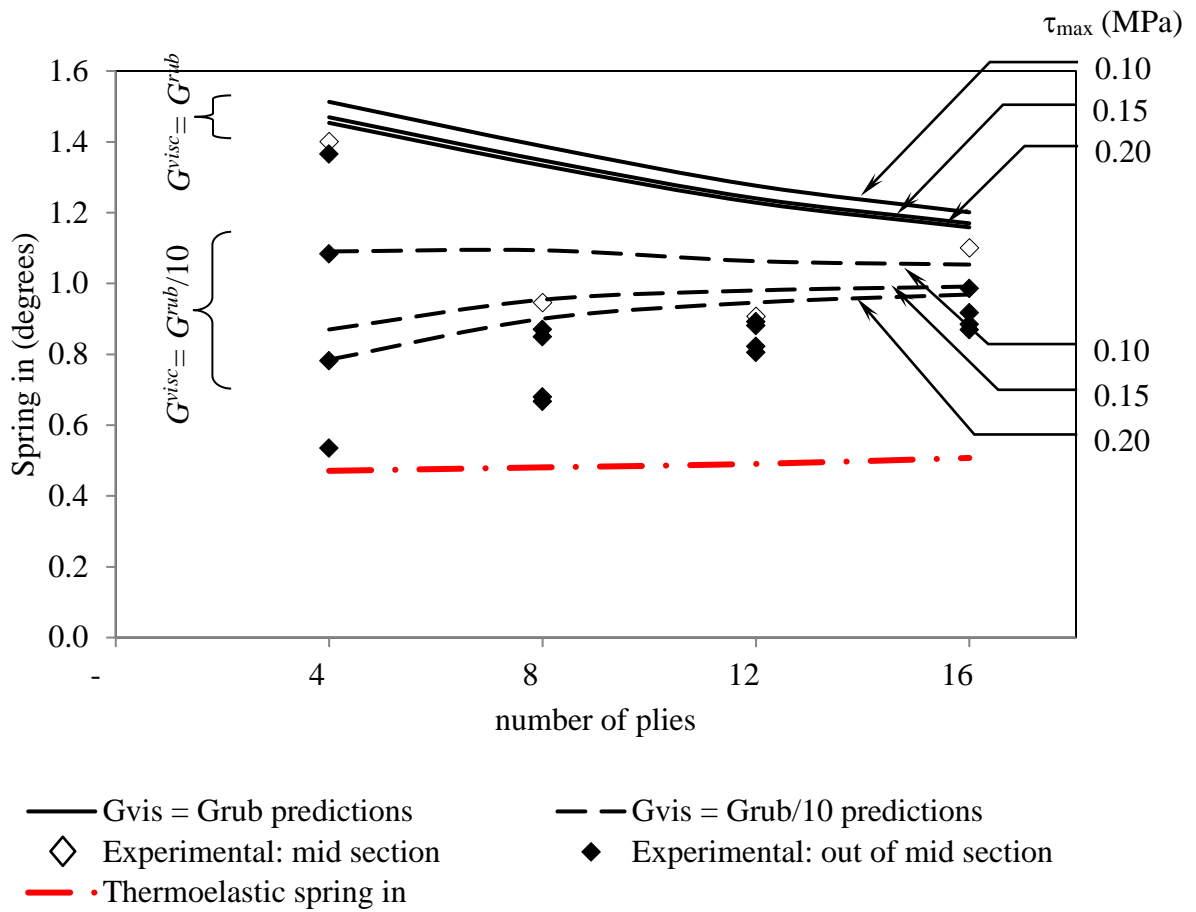


**Figure 12.**Effect of sliding shear stress and viscous shear modulus on spring-in predictions for XP-R15 parts.

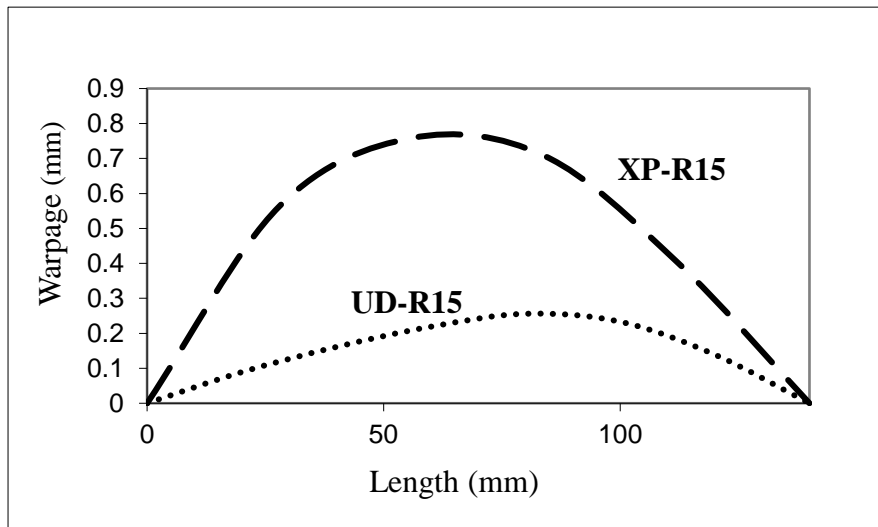


**Figure 13.**Representation of warpage along 3<sup>rd</sup> direction for 4 ply R15 parts.

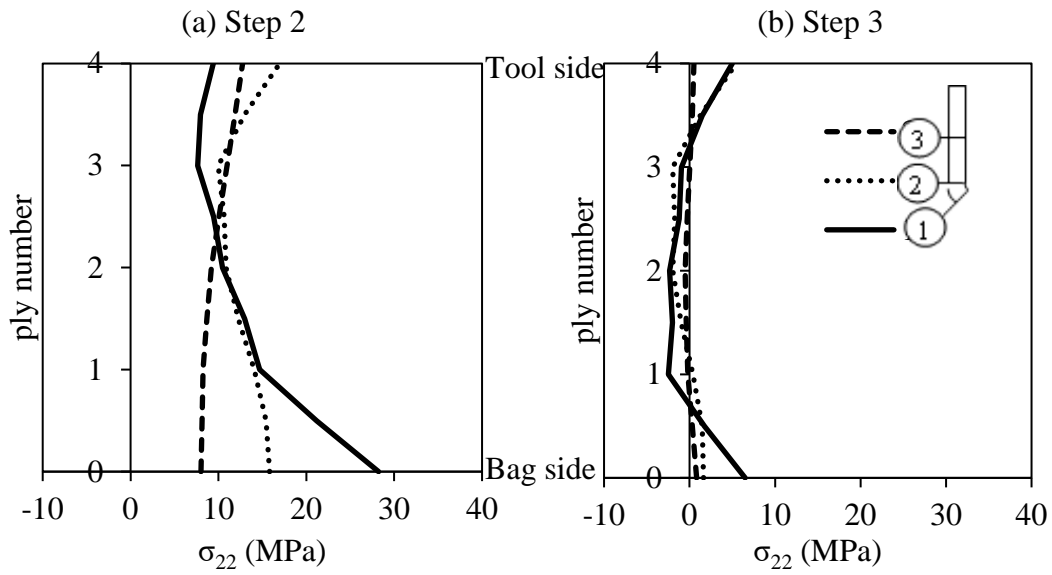


**Figure 14.** Fibre direction stress for UD4-R15 part at the end of (a) 2<sup>nd</sup> step (b) 3<sup>rd</sup> step.

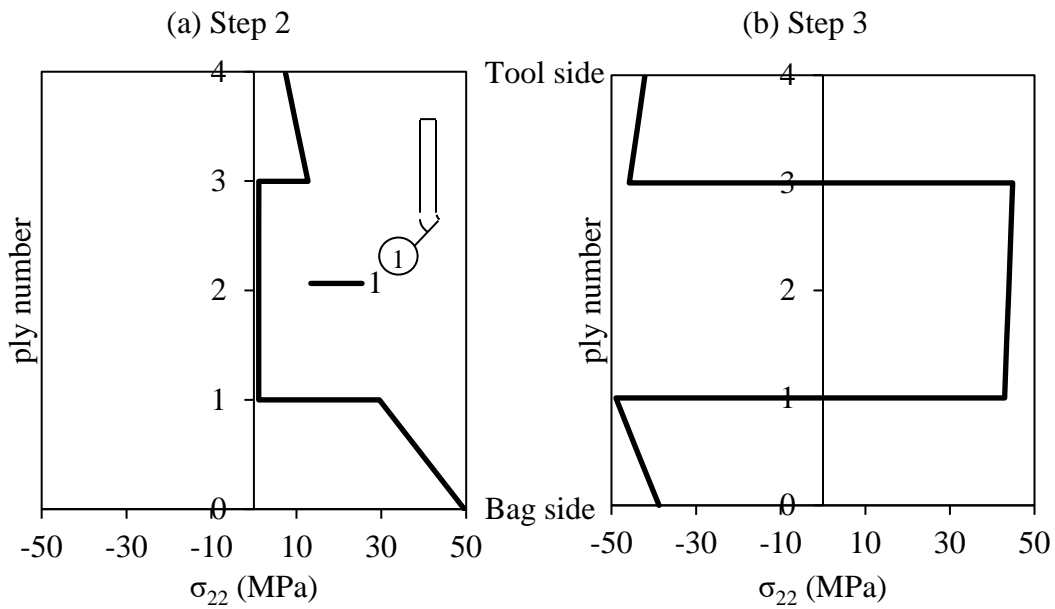


**Figure 15.** Fibre direction stress for XP4-R15 part at the end of (a) 2<sup>nd</sup> step (b) 3<sup>rd</sup> step.

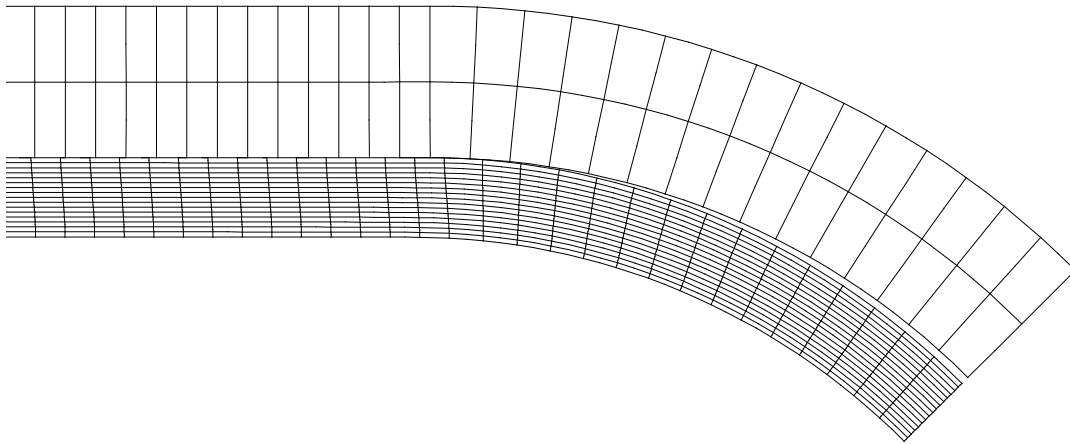


**Figure 16.**Representation of opening at the end of 2<sup>nd</sup> step for 16UD-R15 part.

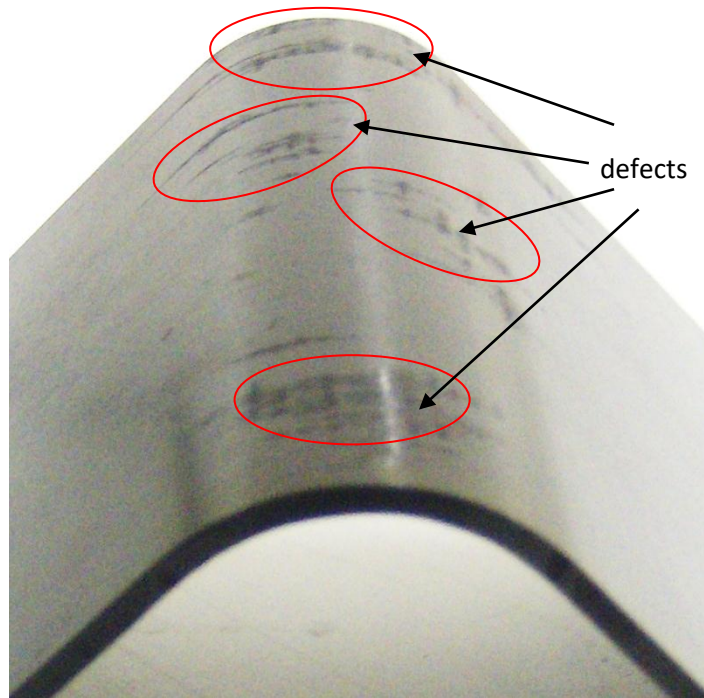


**Figure17.** Surface defects created by separation of part from the tool during manufacturing.

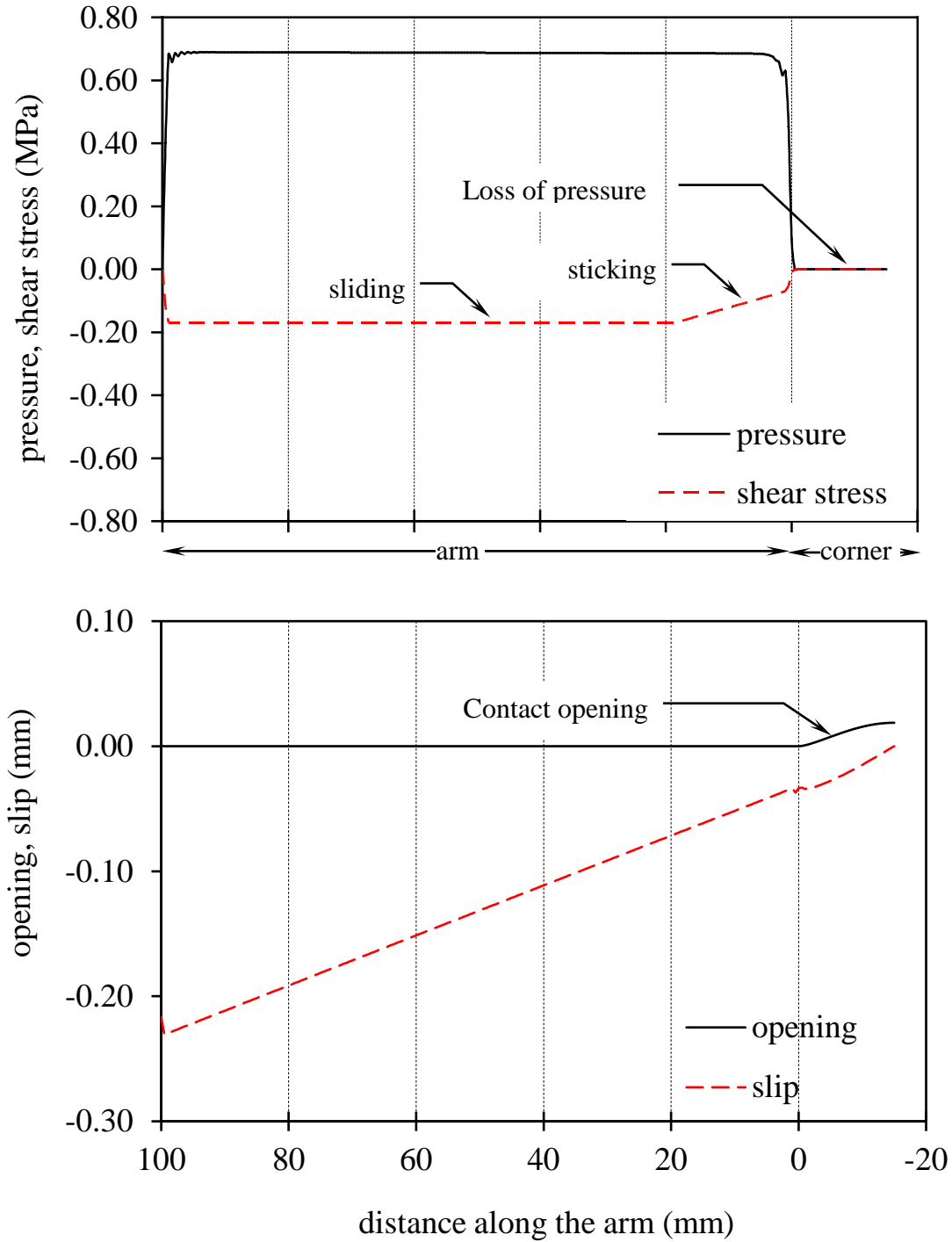


**Figure 18.** Stresses and displacements at the contact interface at the end of the second step for 16UD-R25 part.